Coupled Model of Concentration Polarization and Pore Transport in Crossflow Nanofiltration

Subir Bhattacharjee, Jim C. Chen, and Menachem Elimelech
Dept. of Chemical Engineering, Environmental Engineering Program, Yale University, New Haven, CT 06520

A coupled model of concentration polarization and pore transport of multicomponent salt mixtures in crossflow nanofiltration rigorously predicts local variations of ionic concentrations, flux and individual ion rejections along a rectangular crossflow filtration channel by a coupled solution of the convective-diffusion and extended Nernst-Planck equations. Coupling the pore transport model with the multicomponent convective-diffusion equation in the concentration polarization layer provides a comprehensive understanding of the interplay between concentration polarization and salt rejection. The coupled model is used to predict the local variations of ion rejection, permeate flux and mixture composition in a rectangular crossflow filtration channel for three-component salt mixtures. The total membrane surface concentration of the ions and the ratio of different ions in the mixture (salt ratio) can change considerably along a crossflow filtration channel, and, consequently, cause remarkable variations in intrinsic ion rejections with axial position in the channel.

Introduction

Nanofiltration (NF) membranes with pore sizes in the nanometer range are particularly well suited for removal of polyvalent ions and dissolved organics from aqueous feeds (Mulder, 1991; Raman et al., 1994; Peeters et al., 1998). Advent of these membranes has generated an immense interest in the application of nanofiltration processes for water treatment, clarification of industrial wastewater by removal of dissolved species, and a variety of bioseparations. Considerable attention has been devoted toward understanding the rejection mechanisms of charged (ionic) species by NF membranes (Hijnen et al., 1985; Cwirko and Carbonell, 1989, 1990; Basu and Sharma, 1997; Hall et al., 1997; Hijnen and Smit, 2000), leading to two modeling approaches, namely, nonequilibrium thermodynamic and hydrodynamic models. The macroscopic phenomenological coefficients in these models are often rooted in the microscopic transport phenomena governing the movement of ions through the membrane pores.

A fundamental relationship governing the transport of ionic species through membrane pores is the extended Nernst-Planck equation (Dresner, 1972; Hijnen et al., 1985; Cwirko and Carbonell, 1989; Tsuru et al., 1991c). Insights gleaned from a large body of theoretical development in the area of electrokinetic transport phenomena through capillaries on the basis of the space-charge model (Sasidhar and Ruckenstein, 1981, 1982; Cwirko and Carbonell, 1989; Smit, 1989; Masliyah, 1994; Basu and Sharma, 1997) have led to the formulation of a simplified approach for modeling ion transport through membrane pores. In this approach, one uses a homogeneous one-dimensional (1-D) version of the extended Nernst-Planck equation to analyze the movement of the ions through the membrane pores (Tsuru et al., 1991a,b,c; Wang et al., 1995; Palmeri et al., 1999). Based on these studies, it is now well understood that rejection of ions by membrane pores is a manifestation of the equilibrium partitioning behavior of the ions at the pore-solution interface and the ionic fluxes generated through convective, diffusive, and electrostatic potential driven migration forces.

An integral controlling parameter for ion transport within the pores is the membrane feed solution interfacial concentration, which appears as a boundary condition in the pore transport models. This concentration primarily dictates the intrapore ion concentrations through the partition coefficient (Deen, 1987), and also governs the net ionic fluxes by means of the convective and electrostatic migration terms in the ex-

Correspondence concerning this article should be addressed to M. Elimelech.
Present address of S. Bhattacharjee: Dept. of Mechanical Engineering, 4-9 Mechanical Engineering Building, University of Alberta, Edmonton, Alberta, T6G-2G8, Canada.

tended Nernst-Planck equation. This so-called membrane surface concentration is generally higher than the bulk feed concentration due to concentration polarization (CP) of the rejected solutes (Porter, 1972; Bouchard et al., 1994; Song and Elimelech, 1995; Elimelech and Bhattacharjee, 1998). Moreover, in crossflow membrane filtration units, the membrane surface concentration is known to vary along the channel length (Song and Elimelech, 1995; Elimelech and Bhattacharjee, 1998). Consequently, it is evident that a key boundary condition governing ion transport through the membranes, and, hence, the ionic rejections, will change with location in the filtration channel. In this context, it is surprising to note that most previous models of pore transport either do not account for CP (Tsuru et al., 1991a,b,c; Bowen and Mukhtar, 1996), or resort to a film theory based approach to account for CP (Bowen and Mohammad, 1998).

Use of film approximations to model the CP boundary layer may be applicable to dead-end nanofiltration systems where the extent of CP is assumed to be spatially invariant, but is certainly inadequate for crossflow filtration modules where the extent of polarization varies along the channel length. A further complication arises for multicomponent ionic mixtures typically encountered in nanofiltration processes, where the rejections of the individual components are different (Tsuru et al., 1991c; Peeters et al., 1998, 1999). This engenders a variation of the ionic mixture composition along the channel length. It is, therefore, clearly discernable that concentration polarization and intrinsic membrane rejection are *coupled* phenomena, which must be addressed simultaneously in models of crossflow membrane filtration.

There are, however, no existing models of concentration polarization in crossflow membrane filtration of multicomponent mixtures that consider variations of intrinsic rejection along the filtration channel. In this regard, very few earlier studies even attempt to describe concentration polarization for multicomponent mixtures (Saksena and Zydney, 1997). Keeping in mind that NF operations generally involve ionic mixtures as feed solution, such processes should be analyzed using multicomponent models for concentration polarization. Furthermore, for partially rejecting NF membranes, it is equally important to assess the extent to which individual ions in a mixture are rejected. Thus, a coupled model that simultaneously predicts the local variations of CP, permeate flux, as well as intrinsic and observed rejections for crossflow membrane filtration is necessary to provide a mechanistic insight regarding the performance of crossflow NF processes.

In this article, we describe a rigorous model for simultaneous prediction of local variations of permeate flux and intrinsic and observed rejections for multicomponent ionic mixtures in a rectangular crossflow nanofiltration channel. The model simulates the CP and pore transport phenomena by solving the convective-diffusive equation in the boundary layer and the extended Nernst-Planck equation within the membrane pores, respectively. The two transport models are coupled through the boundary conditions at the membrane/feed-solution interface. A coupled solution of the two models is presented for ternary ionic mixtures. The model predictions depict the coupling between concentration polarization and intrinsic rejection, and the influence of these two phenomena in governing the overall filtration behavior (permeate flux and ion rejection) at various axial positions in a crossflow filtration module.

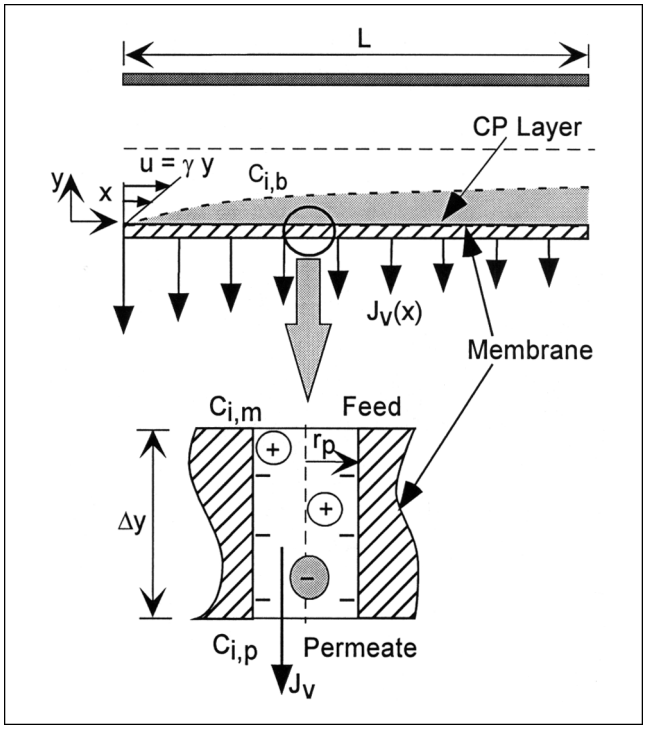

Figure 1. Coupling between the boundary layer transport model for concentration polarization (CP) and the pore transport model.

The two independent models have common boundary conditions given in terms of the membrane surface concentration of the ionic species $C_{i,m}$. In this figure, u represents the axial velocity (along x), J_v represents the local permeate flux, $C_{i,b}$ and $C_{i,p}$ denote the feed bulk and permeate concentrations of the ith ionic species, Δy represents the pore length (membrane thickness), and r_p represents the pore radius.

Mathematical Model

The overall task of simultaneously predicting the permeate flux and rejection of ionic components of a mixture involves a coupled solution of two transport models. The first model describes the transport phenomena in the concentration polarization boundary layer on the feed side adjacent to the membrane, while the second model deals with transport phenomena in the membrane pores. The coupled transport phenomena in crossflow membrane filtration processes are depicted in Figure 1. The model of concentration polarization is applied to the entire filtration channel, yielding local variations of the permeate flux, while at each axial position, the pore transport model provides a detailed analysis of the transport of various ionic species across the membrane pores, yielding the intrinsic rejection of the ionic species. The pore transport behavior at each axial location of the filtration channel is governed by two parameters—the membrane surface concentration of the ions and the permeate flux.

In this section, we first present a multicomponent model of concentration polarization (CP) for noninteracting ionic mix-

tures. The pore transport model is then coupled to the CP model through the membrane surface boundary condition. The coupled solution of the pore transport and CP models provides simultaneous predictions of the permeate flux and observed rejection of the ionic species.

Concentration polarization of multicomponent ionic system

The concentration polarization of the multicomponent ionic system in a crossflow membrane filtration unit is modeled using the steady-state differential material balance for each component as (Bhattacharjee et al., 1999)

$$u\frac{\partial C_i}{\partial x} + J_v\frac{\partial C_i}{\partial y} = \frac{\partial}{\partial y}\left(D_{i,\infty}\frac{\partial C_i}{\partial y}\right) \tag{1}$$

where u is the axial velocity, C_i is the concentration of the ith ion, J_v is the permeate flux, $D_{i,\infty}$ is the diffusion coefficient of the ith ion, and x and y represent the axial and normal coordinate directions, respectively (Figure 1). For simplicity, we assume a linear axial velocity profile $u = \gamma y$, where γ is the shear rate. Such a velocity profile may be safely assumed for nanofiltration of dilute electrolyte solutions as the boundary layer developed will be usually quite thin compared to the channel height, and the solution viscosity will not differ significantly from the pure solvent viscosity. It should be noted that the above model assumes no coupling between the diffusion coefficients of different species and thus is valid for noninteracting solutes. Such an assumption may be satisfactory for dilute ionic systems, although more generalized equations can be developed (Saksena and Zydney, 1997).

The boundary conditions at the membrane channel inlet and the bulk solution are, respectively

$$C_i(0, y) = C_{i,b} \tag{2a}$$

$$C_i(x, \delta) = C_{i,b} \tag{2b}$$

where $C_{i,b}$ is the bulk ionic concentration and δ represents the thickness of the concentration polarization layer. The boundary condition at the membrane surface is (De et al., 1997; Bhattacharjee et al., 1999)

$$R_{i,\text{int}}J_vC_{i,m} = -D_{i,\infty}\left(\frac{\partial C_i}{\partial y}\right) \quad \text{at} \quad y = 0 \tag{3}$$

where $R_{\text{i,int}}$ is the intrinsic rejection of the ionic species i, J_v is the permeate flux, and $C_{i,m}$ is the membrane surface concentration of the ith ionic species. Electroneutrality is maintained throughout the boundary layer, implying

$$\sum_i z_iC_i = 0 \tag{4}$$

where z_i is the valence of the ionic species. Thus, we consider the charge coupling between the ions in the polarized layer through the electroneutrality condition (Eq. 4).

The permeate flux J_v is expressed in terms of the osmotic pressure model (Bhattacharjee et al., 1996, 1999; De et al., 1997)

$$J_v = L_p(\Delta P - \sigma_o\Delta\Pi_m) \tag{5}$$

where L_p is the membrane permeability, ΔP is the applied pressure difference, and σ_o is the osmotic reflection coefficient. The term $\Delta\Pi_m$ denotes the osmotic pressure difference between the membrane surface and permeate. As we are dealing with dilute electrolyte solutions, $\Delta\Pi_m$ is related to the solute concentration difference across the membrane by the linear van't Hoff relationship. In writing Eq. 5 for the permeate flux, we neglect any resistance due to membrane fouling, which is a reasonable assumption for nanofiltration of dilute aqueous electrolyte solutions.

The above model for concentration polarization may be solved to obtain the concentration profiles of different ionic species in a multicomponent mixture and the permeate flux, if independent estimates of the intrinsic rejection of the ionic species are available. The model can serve as a standalone procedure for predicting the *local* variations of permeate flux in a crossflow filtration unit when the ionic species are completely rejected ($R_{i,\text{int}} = 1$), or when the intrinsic rejection is a constant, independent of the physico-chemical parameters governing the separation process. The model, however, cannot be applied to systems where the intrinsic rejection is dependent on the local permeate flux, composition of the salt mixture, and other operating conditions. It is therefore important to assess the extent of coupling between concentration polarization and intrinsic membrane rejection. To achieve this goal, we next present a homogeneous pore transport model for multicomponent salt mixtures to predict the intrinsic ionic rejections.

Transport of ionic mixtures through membrane pores

The governing equation for the steady-state flux j_i of a charged species through membrane pores is the extended Nernst-Planck equation (Dresner, 1972; Tsuru et al., 1991c; Masliyah, 1994; Hall et al., 1997)

$$j_i = -D_{i,m}\frac{\partial c_i}{\partial y} + K_{i,c}c_iJ_v - \frac{z_ic_iD_{i,m}F}{RT}\frac{\partial\psi_m}{\partial y} \tag{6}$$

which incorporates the combined contributions from diffusion, convection, and the electrical mobility of ions. Here, $D_{i,m}$ is the hindered diffusivity of ions in the pores (Deen, 1987), c_i is the molar pore concentration of the ionic species with charge z_i, $K_{i,c}$ is the convective hindrance factor (Deen, 1987), J_v is the permeate flux, F is the Faraday constant, R is the universal gas constant, T is the absolute temperature, and $\partial\psi_m/\partial y$ is the electrical potential gradient along the pore length, which is the driving force for the electrical mobility of the ions. The electrical mobility contribution assumes a constant electric field within the membrane pore and thus requires invoking a no current condition within the membrane

$$I = \sum_i Fz_ij_i = 0 \tag{7}$$

and electroneutrality in the membrane pore

$$\sum_i z_i c_i + X = 0 \tag{8}$$

where X represents the charge density (charge/volume) in the membrane pore matrix (Cwirko and Carbonell, 1989).

Combining Eqs. 6–8, and noting that at steady state $j_i = J_v C_{i,p}$, where $C_{i,p}$ is the concentration of the ith ionic component in the permeate, we obtain

$$\frac{\partial \psi_m}{\partial y} = \frac{J_v \sum_i \frac{z_i}{D_{i,m}} \left(K_{i,c} c_i - C_{i,p} \right)}{\frac{F}{RT} \sum_i z_i^2 c_i} \tag{9}$$

The boundary conditions to Eq. 6 are

$$c_i = c_{i,0} \quad \text{at} \quad y = 0 \tag{10a}$$

$$c_i = c_{i,\Delta y} \quad \text{at} \quad y = -\Delta y \tag{10b}$$

where Δy is the length of the membrane pore (membrane thickness), and $c_{i,0}$ and $c_{i,\Delta y}$ are the intrapore concentrations of the ionic species at the pore entrance and exit, respectively.

The above equations constitute a 1-D model for ion transport within the membrane pores. The ion concentrations in these equations may be construed as average concentrations at any given axial position y within the pore. Such an assumption seems adequate, given the small pore radii (~ 1 nm) encountered in nanofiltration membranes (Cwirko and Carbonell, 1989; Palmeri et al., 1999).

Solution of the extended Nernst-Planck equation provides the ionic fluxes and permeate concentrations corresponding to a given feedside membrane surface concentration and permeate flux J_v. Equation 6 can be solved using appropriate expressions for the hindrance factors and expressions relating the intrapore ion concentrations to the interfacial bulk concentrations.

The restrictive pore size in nanofiltration membranes (~ 1 nm) impedes the convective and diffusive mobility of the ions through the membrane (Deen, 1987; Bowen and Mukhtar, 1996). These effects are incorporated in Eq. 6 through the hindrance factors $K_{i,c}$ and $K_{i,d}$, respectively. In this study, we use the following correlations (Bowen and Mukhtar, 1996)

$$K_{i,c} = \frac{v_i}{J_v} = -0.301 \lambda_i + 1.022 \tag{11a}$$

$$K_{i,d} = \frac{D_{i,m}}{D_{i,\infty}} = -1.705 \lambda_i + 0.946 \tag{11b}$$

where $\lambda_i = r_{i,s}/r_p$, with $r_{i,s}$ and r_p being the ionic species and pore radii, respectively. The convective hindrance factor $K_{i,c}$ represents the ratio of the ionic velocity in the pore v_i to the solvent velocity J_v, while the diffusive hindrance factor $K_{i,d}$ represents the ratio of the hindered diffusivity of the ion in the pore $D_{i,m}$, to the Stokes-Einstein bulk diffusivity of the ion $D_{i,\infty}$. The ionic radii and diffusivities are estimated from the Stokes-Einstein equation

$$r_{i,s} = \frac{RT}{6\pi\mu D_{i,\infty} N_A} \tag{12a}$$

$$D_{i,\infty} = \frac{RT u_i}{|z_i| F} \tag{12b}$$

where μ is the solvent viscosity, N_A is the Avogadro number, and u_i is the ionic mobility (Masliyah, 1994).

Intrapore concentrations at the pore boundaries are related to the interfacial bulk concentrations through partition coefficients. The traditional Donnan partitioning accounts for the electrostatic effects in which the charged membrane will attract counter-ions and repel coions (Tsuru et al., 1991a,c; Donnan, 1995). Here, we also consider steric partitioning of the ions, which results from the finite sizes of the ions (Deen, 1987; Palmeri et al., 1999). The overall partition coefficient may be represented as a superposition of the Donnan and steric effects as (Basu and Sharma, 1997)

$$\phi_i = \frac{c_i}{C_{i,m}} = (1 - \lambda_i)^2 \exp\left(-\frac{z_i F}{RT} \Delta \psi_D \right) \tag{13a}$$

Ideally, the above approximation should be valid when $\lambda_i \ll 1$. The term $\Delta \psi_D$ represents the Donnan potential difference across the membrane. This potential is related to the membrane charge density X and the bulk ion concentrations, and may be eliminated from Eq. 13a by noting that for each ionic species

$$\left[\frac{c_i}{C_{i,m}(1 - \lambda_i)^2} \right]^{1/z_i} = \exp\left[-\frac{F \Delta \psi_D}{RT} \right] = \text{constant} \tag{13b}$$

Finally, considering the membrane electroneutrality condition (Eq. 8), as well as the bulk electroneutrality (Eq. 4), we can evaluate the intrapore ion concentrations from the corresponding membrane surface concentrations.

Solution of the pore transport equations (see next subsection and Appendix A for details) provides the ionic concentrations in the permeate. The results of the pore transport model are expressed in terms of two dimensionless quantities, namely, the intrinsic salt passage and the intrinsic rejection. The intrinsic salt passage is defined as the ratio of the permeate concentration to the feed side membrane surface concentration

$$S_i = \frac{C_{i,p}}{C_{i,m}} \tag{14}$$

whereas the intrinsic rejection is given by

$$R_{i,\text{int}} = 1 - S_i = 1 - \frac{C_{i,p}}{C_{i,m}} \tag{15}$$

Numerical solution of the governing equations

The governing equations for concentration polarization are nondimensionalized and discretized using the method of lines (Zwillinger, 1989; Bhattacharjee et al., 1999). The resulting system of coupled ODEs is then solved numerically using a backward difference predictor-corrector method (Petzold, 1982). For an n-component system, the transport of $(n-1)$ components is derived from the solution of the convective-diffusion equation, while the nth component follows from the bulk electroneutrality condition. The numerical solution of the pore transport equations is described in Appendix A.

The overall model couples the pore transport model with the CP model by the intrinsic rejection and concentration values that appear in their respective boundary conditions. The CP model requires input of the membrane intrinsic rejection $R_{i,\text{int}}$ in Eq. 3, which is derived from the solution of the pore transport model. In turn, the pore transport model requires for its boundary conditions the intrapore concentration $c_{i,0}$ at the pore entrance in Eq. 10a, which is determined from the solution of the CP model and the partition coefficient (Eq. 13). The coupling between the two models thus requires an iterative solution procedure as outlined in Figure 2. A self-consistent iterative solution involving the two transport models yields the rigorous concentration profiles throughout the system, the permeate flux, and the observed rejection of the ionic components, given by

$$R_{i,\text{obs}} = 1 - \frac{C_{i,p}}{C_{i,b}} \tag{16}$$

We emphasize here that the coupled model provides the intrinsic and observed rejections, as well as the permeate flux as *local* quantities that depend on the axial position in the membrane filtration unit.

Results and Discussion

The coupled model of concentration polarization and pore transport presented in the previous section provides a self-consistent procedure for predicting all the parameters of interest in nanofiltration processes involving multicomponent salt mixtures. These parameters include the membrane surface concentration of the ionic species, the permeate flux, and the observed and intrinsic rejection of the ions. Furthermore, these quantities are predicted for every axial location in the crossflow filtration channel. The operating conditions and physico-chemical properties used in the model predictions presented in this article are listed in Table 1. Typical operating parameters are the applied pressure, crossflow velocity or the shear rate, bulk feed concentration, and the channel length. The fundamental membrane properties required as inputs to the model are pore radius, membrane thickness, porosity, and membrane charge density. Once a specific salt mixture is used, the associated fundamental properties of the various ions in the mixture can also be easily determined. The pertinent properties of the ions in the representative $NaCl/Na_2SO_4$ mixture used in this investigation are given in Table 2.

To facilitate understanding the influence of different physico-chemical conditions on the rejection behavior, it is

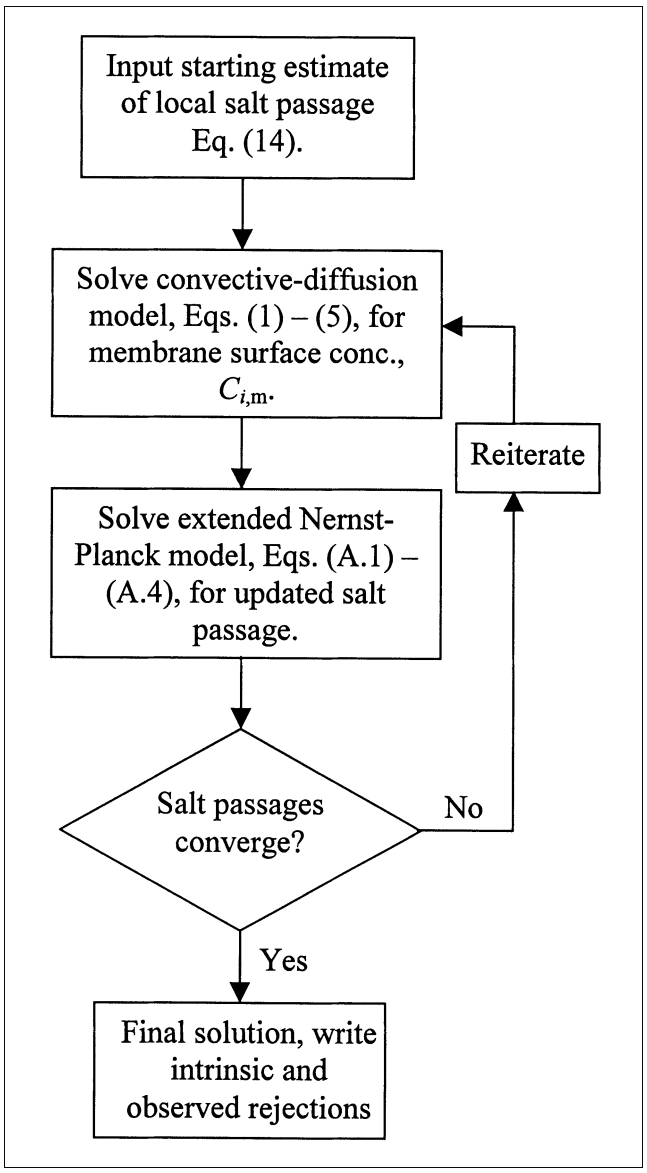

Figure 2. Numerical solution procedure for the coupled model to simultaneously solve extended Nernst-Planck and convective-diffusion equations.

Table 1. Properties of the System Used in Simulations

Salt mixture	NaCl and Na_2SO_4
Bulk salt concentration,* C_T	1 mM
Channel length, L	0.2 m
Membrane thickness (pore length), Δy	10 μm
Membrane charge density, X	-10 mEq
Pore radius, r_p	1 nm
Porosity, α	0.46
Permeability, $L_p = \alpha r_p^2/(8\mu\Delta y)$	6.45×10^{-12} m·Pa^{-1}·s^{-1}
Shear rate, γ	600 s^{-1}
Viscosity, μ	0.891×10^{-3} Pa·s
Pure solvent flux, $L_p\Delta P$	1×10^{-5} m·s^{-1}
Temperature, T	298 K

*Bulk salt concentration is defined as the total molar concentration of the salts NaCl and Na_2SO_4. If the fraction of Cl^-, x_{Cl^-}, in Eq. 18 is additionally specified, all the ionic concentrations can be determined from C_T and x_{Cl^-}.

Table 2. Fundamental Properties of Ions Used in This Study

	Na^+	Cl^-	SO_4^{2-}
Charge, z_i	+1	−1	−2
Ionic mobility, u_i $(m^2 \cdot V^{-1} \cdot s^{-1})$	5.19×10^{-8}	7.91×10^{-8}	8.29×10^{-8}
Diffusivity, $D_{i,\infty}$ $(m^2 \cdot s^{-1})$	1.33×10^{-9}	2.03×10^{-9}	1.06×10^{-9}
Radius, $r_{i,s}$ (nm)	0.184	0.120	0.231

often necessary to perform the simulations corresponding to a fixed permeate flux. The pure water flux of a given membrane is expressed as the product of the permeability and the applied pressure. In this study, the membrane permeability is written in terms of the geometric properties of the membrane as (Bhattacharjee et al., 1996)

$$L_p = \frac{\alpha r_p^2}{8\mu\Delta y} \tag{17}$$

where α is the membrane porosity. Hence, the permeability will change when the pore length or the pore radius changes. To obtain consistent sets of results corresponding to different membrane geometric properties, the applied pressure was adjusted to yield the same pure solvent flux for different membrane permeabilities. It is also worth mentioning at the outset that the osmotic reflection coefficient in Eq. 5 was considered as 1 in all the computations. The resulting error in the estimates of the permeate flux should be negligible since we are dealing with dilute salt solutions and the osmotic pressure term in Eq. 5 is negligible compared to the applied pressure in all subsequent calculations.

In this section, we will present simulation results based on the coupled model for a ternary mixture of NaCl and Na_2SO_4 to illustrate the main features of the developed model. The primary aim will be to highlight the coupling between concentration polarization and pore transport of the ions, which leads to local variations of the ion rejections along the crossflow channel. Following this, the manifestation of such variations in rejection on the overall separation efficiency and the performance of the filtration system will be discussed.

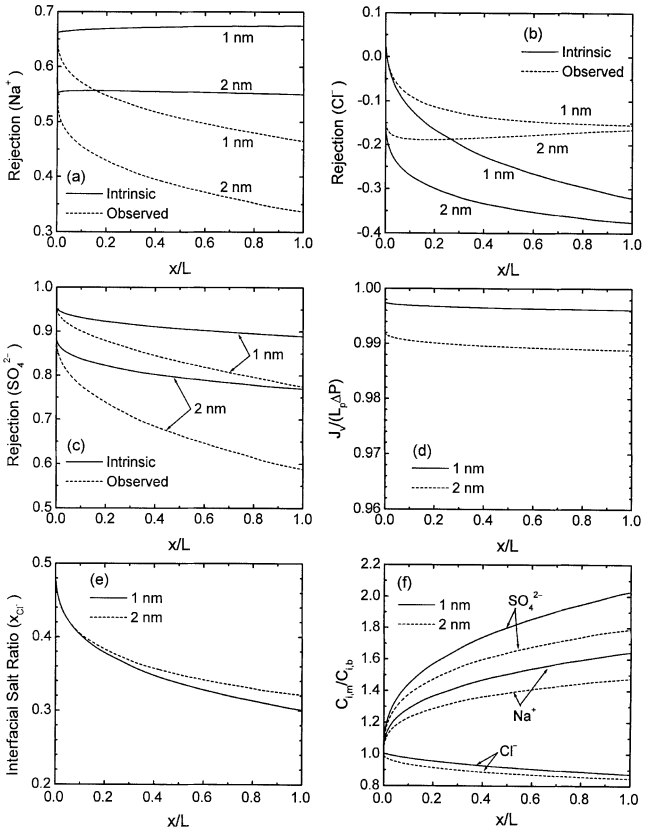

Figure 3. Data from solution of the coupled model, focusing the dependence on axial position along the membrane channel.

The simulations correspond to two pore radii of 1 nm and 2 nm, and a bulk solution Cl^- ratio (x_{Cl^-}) of 0.5, while all other conditions and parameters are fixed according to Tables 1 and 2. In all the figures, the different quantities are predicted for different scaled axial locations (x/L) in the filtration channel. (a)–(c) intrinsic and observed rejections of sodium, chloride, and sulfate ions, respectively; (d) the permeate flux scaled with respect to the pure solvent flux; (e) the ratio of the Cl^- ions (x_{Cl^-}) in the mixture at the membrane surface (Eq. 18); (f) the scaled membrane surface concentrations of the three ions (sulfate, sodium, and chloride).

Ion rejection, permeate flux, and mixture composition along a crossflow filtration channel

Figure 3 depicts simulation results using the coupled model for a 0.2 m long rectangular crossflow channel that illustrate the dependence of the ionic rejections, permeate flux, and membrane surface concentrations of the ions on the axial position. This set of results is based on the conditions specified in Tables 1 and 2 and was obtained for two pore sizes of 1 nm and 2 nm with the pure solvent flux fixed at 1×10^{-5} m/s. The simulations were performed for a $NaCl/Na_2SO_4$ mixture with a bulk Cl^- fraction of 0.5, which is defined as

$$x_{Cl^-} = \frac{[Cl^-]}{[Cl^-] + [SO_4^{2-}]} \tag{18}$$

Figures 3a–3c show the variations of the intrinsic and observed rejections with scaled axial position (x/L) in the filtration channel for the three ions (sodium, chloride, and sulfate, respectively). The intrinsic rejection of Na^+ increases slightly with axial distance whereas the observed rejection of the ion decreases. For Cl^-, we observe negative values of rejection in downstream channel locations for both pore sizes. The negative rejection implies that the Cl^- ions are preferentially transported through the membrane pores, and that the permeate solution is more enriched in this ion compared to the feed solution. Interestingly, for the larger pore (2 nm), the observed rejection of chloride ions appears to increase with axial distance. The SO_4^{2-} coions exhibit highest rejection among the three components of the salt mixture due to its divalent charge. For all the ions, the rejection decreases with increasing pore radius, showing the model's sensitivity to finite ion and pore sizes. Figure 3d shows the corresponding scaled permeate fluxes for the two pore sizes. Although the extent of flux decline from the pure solvent flux is negligible, we observe a slight decrease in the scaled permeate flux with

increasing pore size. The variation of the permeate flux with axial position appears to be quite small. In Figure 3e, we plot the Cl^- ratio (Eq. 18) in the mixture at the membrane surface against the scaled axial position. This ratio changes considerably with axial distance, indicating that the mixture composition at the membrane surface varies significantly from that at the channel entrance. The mixture is generally enriched with the highly rejected components at downstream locations. Finally, in Figure 3f, the variations of the scaled membrane surface concentrations of the different ionic species with axial position are shown. Among the three components, the concentration buildup of sulfate is most marked followed by that for sodium. The concentration of Cl^- slightly decreases at downstream channel locations, which is commensurate with the negative rejection of this ion. The concentration buildup of the different ions appears to follow the trends in their respective rejection behaviors.

An interesting feature of these results is that we do not observe any qualitative similarities in the trends of the intrinsic and observed rejections of the ions in Figures 3a–3c. Notably, for Na^+, the intrinsic rejection appears to slightly increase, while the observed rejection decreases at downstream locations in the channel (Figure 3a). These results can be explained by noting the variation of the salt ratio along the axial direction (Figure 3e). In downstream locations, the solution near the membrane surface has a higher proportion of sulfate ions, and, correspondingly, requires a higher retention of the sodium ions to satisfy local electroneutrality. Consequently, the intrinsic rejection of Na^+ increases with axial distance. However, it should also be noted that at downstream locations the intrinsic rejection of sulfate ions decreases, causing a higher passage of SO_4^{2-} through the membrane. Since each sulfate ion needs to be associated with two sodium ions to satisfy electroneutrality in the permeate, a larger amount of Na^+ will be transferred to the permeate solution, thereby increasing the Na^+ concentration in the permeate. As the observed rejection is determined on the basis of a fixed bulk sodium ion concentration, the observed rejection of Na^+ will therefore decrease with axial distance. A similar explanation also dictates the intrinsic and observed rejection behavior of chloride ions.

These representative results indicate the broad range of information that can be obtained regarding the performance of a crossflow nanofiltration process on the basis of fundamental physico-chemical parameters listed in Tables 1 and 2. These simulations also highlight some of the key features of the present methodology, and their influence on the separation of multicomponent ionic mixtures. First, the incorporation of the finite ion size effects in the hindered transport parameters and the partition coefficients (Eqs. 11 and 13, respectively) lead to the dependence of these results on the pore size. In the absence of these steric parameters, the basic Nernst-Planck equations along with Donnan partition coefficients would fail to provide the pore-size dependence of the intrinsic rejection. Secondly, these results illustrate the intimate coupling between the concentration polarization effects and the intrinsic rejection of the ionic species, which leads to significant variations of the rejections, salt ratio, and membrane surface concentrations of the ions with axial position in the channel.

Necessity of a coupled model: comparison with fixed intrinsic rejection CP model

To further highlight the necessity of a coupled prediction of concentration polarization and pore transport, we consider a scenario in which we solely employ the CP model with fixed independent estimates of the intrinsic ionic rejections in Eq. 3. In using the fixed intrinsic rejection CP model, it was assumed that such rejections are independently evaluated from the pore transport model on the basis of the bulk solution concentration and salt composition. Using these assumptions, predictions of the product (permeate) concentrations were obtained for different pure water fluxes and a pore radius of 1 nm, keeping all other parameters fixed (corresponding to those given in Table 1).

Variations of the permeate composition, represented as $\sum_i z_i C_{i,p}$, with the scaled axial distance from the channel entrance are shown in Figure 4. We note that the ordinate should be zero at all locations in order to satisfy electroneutrality in the permeate solution. Thus, the results in Figure 4 provide an estimate of the deviation from electroneutrality. Clearly, the constant intrinsic rejection CP model *violates* a fundamental physical constraint, namely, the electroneutrality in the permeate solution, at every downstream location in the filtration channel. The magnitude of the error increases with increasing permeation velocity.

This physically erroneous behavior stems from the fact that this model fails to account for the coupling between concentration polarization and the pore transport behavior of the ions. In fact, a constant intrinsic rejection CP model can ensure electroneutrality in the permeate solution only when the intrinsic rejection of all the ionic species is equal or when the membrane surface mixture composition and ionic concentrations do not change with axial position in the crossflow filtration channel. Because these conditions cannot usually be satisfied, application of a model that accounts for the local variations in the intrinsic rejection seems to be the only alternative. This was one of the primary concerns that led to the development of the present coupled model for multicomponent salt mixtures. In contrast to the constant intrinsic rejection CP model, the coupled model self-consistently assures electroneutrality at every point in the computational domain, including the permeate solution. Further discussion of this important point will follow later.

Influence of bulk mixture composition on observed rejection

On the basis of the above discussion, it becomes apparent that one of the key parameters governing ionic rejection that changes considerably along the crossflow filtration channel is the mixture composition. Here, we further elucidate the influence of the mixture composition on ionic rejections. The mixture composition can be expressed in terms of the fraction of a specific coion, as given in Eq. 18. In the case of a mixture of NaCl and Na_2SO_4, the ratio of the more permeable coion (Cl^-) to the less permeable coion (SO_4^{2-}) will be instrumental in dictating the rejection behavior. In Figure 5, local variations of the observed rejection of the three ions for different values of the Cl^- ratio in the bulk feed mixture are shown. A small value of x_{Cl^-} will signify a salt solution predominantly containing Na_2SO_4, while large values of this ra-

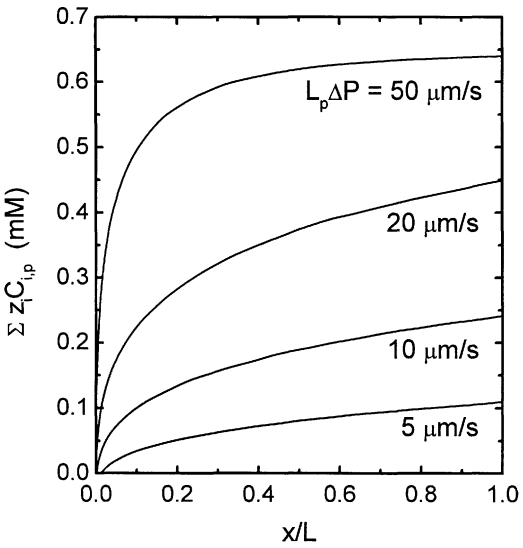

Figure 4. Variation of the product (permeate) charge $\Sigma z_i C_{i,p}$ with axial distance obtained using the constant intrinsic rejection CP model.

For electroneutrality of the permeate solution, the sum must be zero. The simulations correspond to conditions specified in Table 1 with a pore radius of 1 nm and $x_{Cl^-} = 0.5$ in the bulk solution.

tio will imply a solution containing mostly NaCl. It is observed that the sulfate ions are highly rejected for all values of x_{Cl^-}, with the rejection increasing with larger x_{Cl^-} (Figure 5a). A similar behavior is observed for the chloride ions. In this case, the Cl^- rejection is negative for small values of x_{Cl^-}, gradually reaching the positive rejection domain for $x_{Cl^-} > 0.7$ (Figure 5b). The rejection of the counterion (Na^+) shows an opposite trend with increasing x_{Cl^-} (Figure 5c). For small x_{Cl^-}, the rejections are higher, closely following the trends of SO_4^{2-}, whereas for large values of x_{Cl^-}, the rejection of Na^+ follows the corresponding behavior of the Cl^- ions. This suggests that for charged membranes, the transmembrane transport of the counterions is largely governed by the transport behavior of the dominant (highly rejected) coions. These simulations further indicate that the transport behavior for single salt systems are recovered in the limit of $x_{Cl^-} = 0$ (Na_2SO_4) and $x_{Cl^-} = 1$ (NaCl).

Coupled influence of salt concentration and composition on intrinsic rejection

The variation of the observed rejection with axial position in the channel is related to the corresponding changes in the intrinsic rejection of the ions. It is evident that such variations are engendered primarily by the local variations in the mixture composition, as well as the total ion concentrations at the membrane surface. Here, a detailed analysis of the coupled influence of the two parameters on the intrinsic salt rejection is presented.

The influence of the membrane charge density on the extent of ion rejection is affected by the total ion concentration in the bulk solution. This is due to the increased charge screening at higher electrolyte concentrations and the corresponding reduction in the Donnan exclusion effects. To assess the combined influence of membrane charge density and electrolyte concentration on the intrinsic rejection, we employ a dimensionless parameter, defined as the charge number

$$Ch = \frac{\frac{1}{2}\sum_i z_i^2 C_{i,m}}{|X|} \tag{19}$$

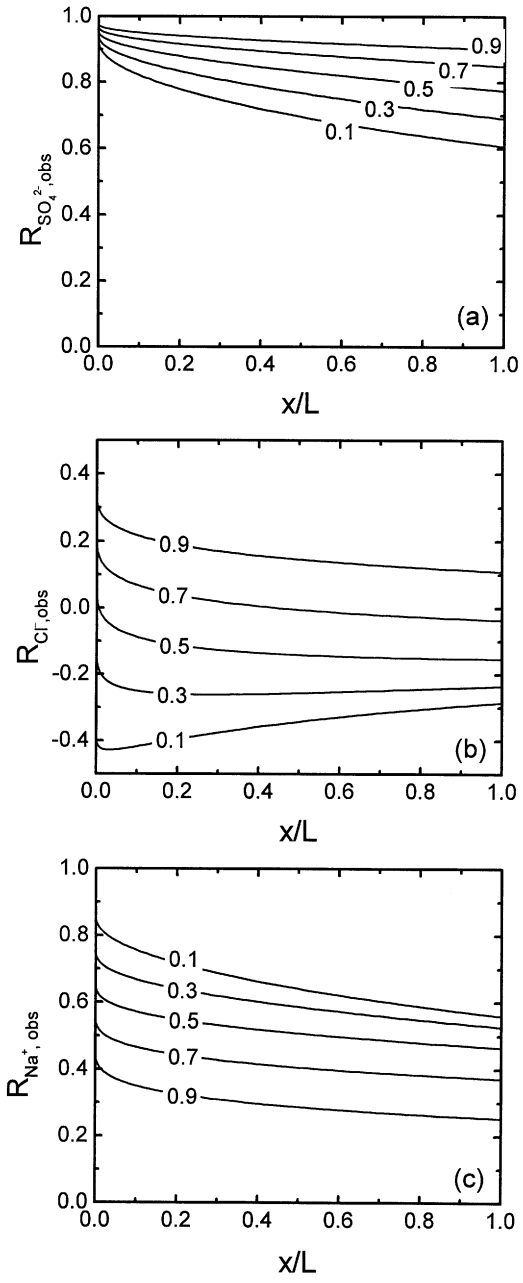

Figure 5. Influence of the bulk Cl^- ratio (Eq. 18) on axial variations of the observed ion rejections.

All operating conditions are given in Table 1. The Cl^- ratio corresponding to each curve is indicated in the figure. The figures, from top to bottom, represent the rejections of (a) sulfate, (b) chloride, and (c) sodium ions.

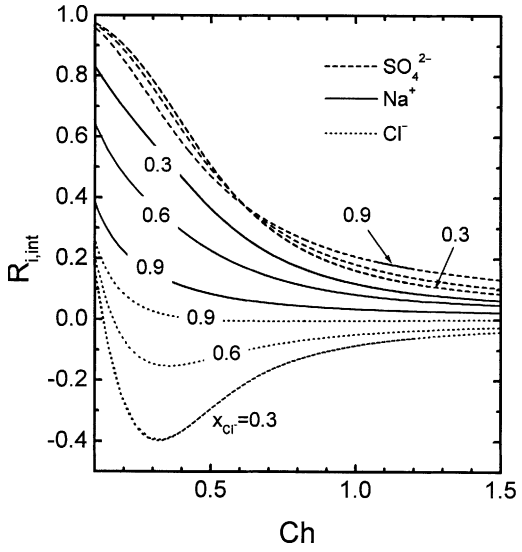

Figure 6. Variation of membrane intrinsic rejection with charge number considering only pore transport mechanisms (that is, no CP effects) for a $NaCl/Na_2SO_4$ system.

The calculations were performed for a pore radius $r_p = 2$ nm and a pure solvent flux of 1×10^{-5} m/s. All other conditions are listed in Table 1. The results are shown for three different values of the bulk Cl^- ratio. The charge number is determined using different combinations of membrane charge density and solution ionic strength.

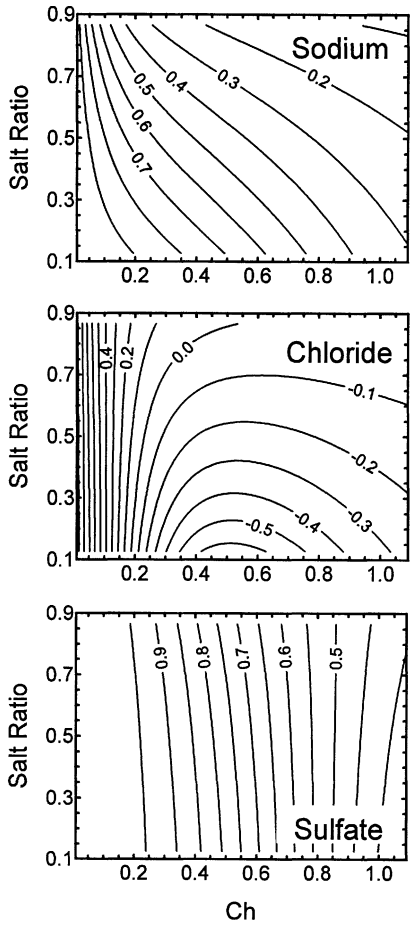

Figure 7. Contours of constant intrinsic rejection plotted on the phase plane comprising the charge number (*Ch*) and the salt ratio (x_{Cl^-}).

The figures map the intrinsic rejection of sodium, chloride, and sulfate ions, respectively, from top to bottom. The simulations are obtained using the pore transport model (that is, no CP effects) employing a pore size of 1 nm. Other conditions are as specified in Table 1. The charge number was varied by changing the membrane charge density, while keeping the bulk salt concentration fixed at 1 mM.

This dimensionless number represents the ratio of the interfacial ionic strength of the electrolyte (that is, at the membrane solution interface) and the magnitude of the membrane charge density. Smaller values of this number $Ch \ll 1$ will imply a rejection behavior governed by Donnan effects, since the membrane charge cannot be effectively screened by the low concentration of the ions. When $Ch > 1$, the rejection will predominantly be governed by steric effects, as the membrane charge is considerably screened by the high electrolyte concentration.

The influence of the charge number on the intrinsic rejection behavior is first assessed solely on the basis of the pore transport model. Figure 6 depicts the variations of the intrinsic ion rejections with the charge number for three different bulk Cl^- ratios. These results were obtained for a pore radius of 2 nm and a permeate flux of 1×10^{-5} m/s assuming no concentration polarization. The feedside interfacial concentration and the membrane charge densities were varied to obtain different values of *Ch*. Notably, for a fixed Cl^- ratio, we observe a unique dependence of the individual ion rejections on the charge number. That is, the rejection remains the same for different combinations of interfacial salt concentration $C_{i,m}$, and membrane charge density X as long as they yield the same *Ch* value according to Eq. 19. For low Cl^- ratios, a deep minimum in the Cl^- rejection near $Ch = 0.33$ is obtained. This number roughly corresponds to the ionic strength where the concentration of the counterions equals the membrane charge density. The depth of the minimum diminishes with increasing Cl^- ratio, and for $x_{Cl^-} = 0.9$, the rejection of Cl^- decays monotonically with increasing *Ch*. With increasing *Ch*, the onset of charge screening mitigates the electrostatic interactions that cause negative rejection of Cl^-, and for relatively large values of *Ch*, the rejection behavior is governed by steric interactions. The variation of sulfate rejection with *Ch* appears to be the least affected by the Cl^- ratio.

The coupled influence of the salt ratio and the charge number on the intrinsic rejection of the ions is mapped as contours of constant intrinsic rejection in Figure 7. These results were obtained for a pore radius of 1 nm and a pure solvent flux of 1×10^{-5} m/s using solely the pore transport model (that is, without considering CP effects). Here, the variations of the charge number are simulated by fixing the total mixture concentration at 1 mM while varying the membrane charge density. The intrinsic rejections of all the ions decrease considerably when the charge number increases. The chloride rejection becomes positive only when $Ch < 0.2$ irrespective of the salt ratio. Under these conditions, the ion transport behavior is dominated by Donnan exclusion effects,

and the rejection of both sodium and sulfate will be considerably high. The figure provides a facile means for studying the variation of the intrinsic rejection of the ionic species along the crossflow filtration channel. We note that keeping the salt ratio fixed, if the charge number is increased, the intrinsic rejections of both Na^+ and SO_4^{2-} will decrease due to charge screening. On the other hand, keeping the charge number fixed, if the salt ratio is decreased, the intrinsic rejection of both sodium and sulfate ions increases slightly. The same observations also apply to Cl^- for $Ch < 0.2$. However, for larger values of Ch, lowering x_{Cl^-} will generally result in a decrease in the rejection of the ion.

As the membrane surface concentrations of the ions change with axial position in the filtration channel due to CP, the charge number and the ratio of different ions in the mixture will vary with channel length. A qualitative understanding of the implications of axial position dependence of Ch and x_{Cl^-} on the ion rejections can be obtained on the basis of Figure 7. Since SO_4^{2-} has a higher rejection and buildup at the membrane surface for a negatively charged membrane, the parameter x_{Cl^-} will generally decrease as one moves along the axial direction in the filtration channel. The overall ionic strength of the solution at the membrane surface will however increase axially due to concentration buildup of the sulfate and sodium ions, causing a net increase in the charge number. Both increasing Ch and decreasing x_{Cl^-} will usually result in lowering the intrinsic rejection of the coions. The rejection of the counterions will, on the other hand, evolve from a competition between the two processes, as decrease in x_{Cl^-} will tend to raise the rejection of Na^+ while increase in Ch will lower its rejection. Quite often such a competition will result in a nearly constant intrinsic rejection of the counterion. This observation is also supported by the relatively small variation of the intrinsic rejection of Na^+ in Figure 3a.

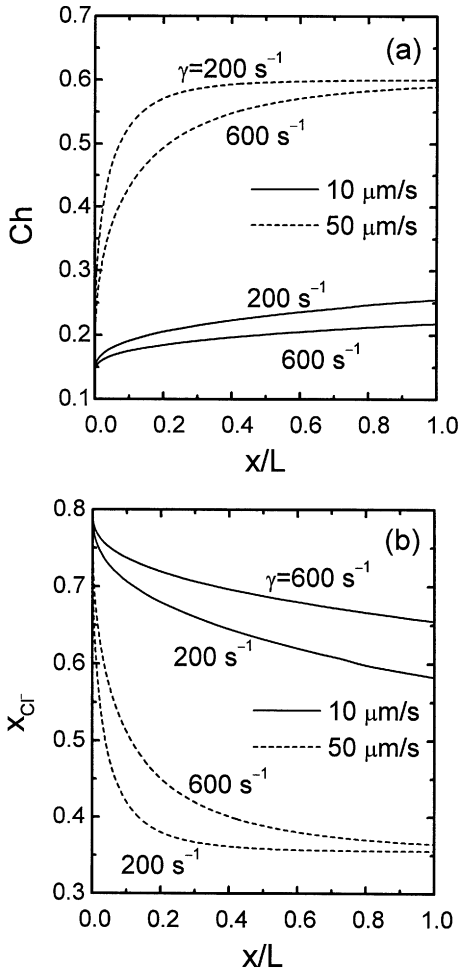

Figure 8. Variation of (a) charge number and (b) Cl^- ratio at the membrane surface with scaled axial distance for different combinations of pure solvent flux and shear rate.

The different fluxes correspond to different operating pressures. The membrane charge density is fixed at -10 mEq/L, while the inlet feed salt concentration in the channel was 1 mM. The results were obtained for a pore radius of 1 nm and $x_{Cl^-} = 0.8$ in the bulk solution. All other conditions are given in Table 1.

Influence of operating conditions on ion rejection

From the foregoing discussion, it is apparent that Ch and x_{Cl^-} are the two primary parameters that influence the intrinsic ion rejections. We now investigate how the charge number and salt ratio change with axial position in a crossflow filtration unit due to concentration polarization under typical operating conditions for nanofiltration processes. Tracking the variation of these two parameters with axial position in a crossflow filtration channel for different operating conditions will lead to an assessment of the rejection behavior of a given crossflow nanofiltration process. Figure 8 shows the variations of the interfacial charge number and the Cl^- ratio with the axial position in the filtration channel for different pure water fluxes (10 and 50 μm/s) and shear rates (200 and 600 s^{-1}). The influence of these hydrodynamic conditions on CP effects are evident from the axial variations of Ch. For a given flux, axial variations of the charge number and Cl^- ratio are less severe at higher shear rates due to lower accumulation of the ions at the membrane surface. At high fluxes and low shear rates, CP effects are enhanced causing significant solute accumulation, and thus there is a rapid increase in Ch along the membrane channel. The highly rejected SO_4^{2-} ions exhibit the greatest extent of CP and thus the Cl^- ratio rapidly decreases in the downstream direction. At high fluxes and low shear rates, a nearly constant solution composition at the membrane surface is attained after relatively short axial distances ($x/L > 0.2$). These calculations were performed using a membrane charge density of -10 mEq/L and a feed bulk concentration of 1 mM. Consequently, $Ch < 1$ in all these results, indicating that charge (or Donnan) exclusion effects will govern the rejection of the ions. Under these conditions, it is expected on the basis of Figure 7 that the intrinsic rejection of the ions will change gradually with axial position for the lower flux, but will rise sharply for $x/L < 0.2$ and become nearly constant thereafter for the higher flux and the lower shear rate.

Variations in the intrinsic ion rejections along the filtration channel owing to the axial position dependence of the membrane surface charge number and Cl^- ratio are depicted in Figure 9. These results correspond to the simulations shown in Figure 8 for the lower shear rate ($\gamma = 200\ s^{-1}$). While the

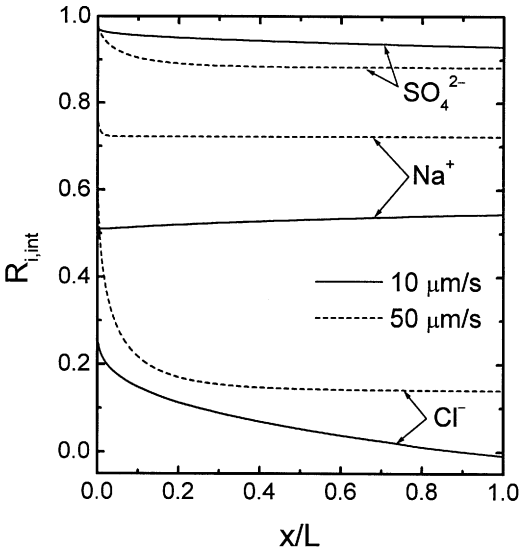

Figure 9. Variation of the intrinsic rejection of sulfate, sodium and chloride as a function of axial position corresponding to a shear rate of 200 s^{-1} for the two permeate fluxes.

All other conditions are the same as in Figure 8.

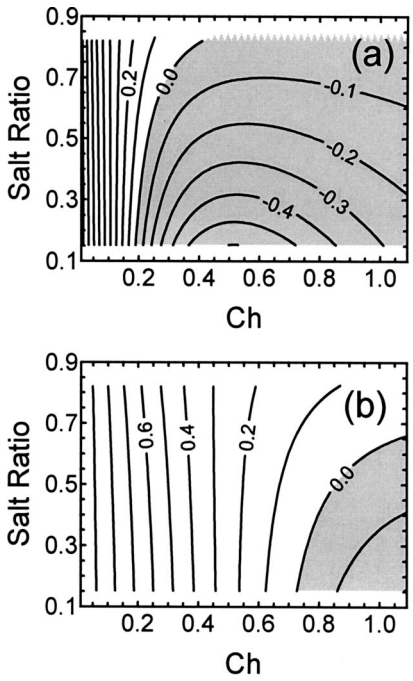

Figure 10. Contours of constant intrinsic rejection of Cl^- ions on the phase plane formed by the charge number and the salt ratio for (a) J_v = 10 μm/s and (b) J_v = 50 μm/s.

All other conditions are the same as in Figures 8 and 9. These results, as in Figure 7, were obtained solely on the basis of the pore transport model (that is, no CP effects). Shaded regions represent negative intrinsic Cl^- rejection.

intrinsic rejection of SO_4^{2-} decreases upon increasing the permeate flux, the corresponding rejections of Na^+ and Cl^- increase. Furthermore, for the higher flux (dashed lines), the intrinsic rejections of all the ions decrease sharply for $x/L < 0.2$ and becomes nearly constant for $x/L > 0.2$. Among the three ions, the rejection of Cl^- varies with axial position most prominently. For low fluxes, the Cl^- rejection decreases gradually with increasing axial distance, attaining negative values toward the end of the channel. The rejection of Cl^- at the higher flux, however, attains a constant positive value after a short downstream distance. Comparing these trends with the corresponding results in Figure 8 shows that a constant intrinsic rejection is attained when both the charge number and Cl^- ratio become independent of axial position.

An important observation from Figures 8 and 9 is that for higher permeate fluxes, the intrinsic rejections of the coions become nearly independent of the axial position. This leads us to study the coupled influence of the permeate flux and the ion exclusion mechanisms on the intrinsic rejection. In Figure 10, the intrinsic rejection of Cl^- is mapped for different combinations of Ch and x_{Cl^-} corresponding to the two values of permeate flux used in the simulations of Figures 8 and 9. While the Cl^- rejection decreases sharply with increasing Ch at the lower flux (Figure 10a), attaining negative values for $Ch > 0.2$, the rejection of this ion decreases more gradually with increasing Ch at the higher flux (Figure 10b). For a fixed Ch, the Cl^- rejection shows very little dependence on x_{Cl^-} at the higher permeate velocity. Furthermore, increasing the permeate flux, while keeping the charge number constant, results in an increase in Cl^- rejection. This behavior is corroborated by the Cl^- rejections shown in Figure 9, and is primarily due to the fact that higher permeate fluxes cause more severe CP, resulting in a higher interfacial charge number. This enhances the charge screening effects, causing the rejection behavior to be governed by steric mechanisms.

The preceding discussion clearly demonstrates the paramount importance of concentration polarization on the intrinsic ion rejections in a crossflow nanofiltration unit. Since the extent of concentration polarization is governed by a combination of crossflow shear rate, operating pressure (permeate flux), and bulk solution concentration, these parameters will also dictate the variations of intrinsic ion rejections along the filtration channel. Higher shear rates will tend to lower the extent of CP, causing a relatively gradual axial variation of the intrinsic rejections. Increasing the operating pressure will result in enhanced CP effects due to the higher permeation velocity, which in turn, can induce dramatic changes in intrinsic rejection. It should be noted that the flux decline associated with the system considered here is quite negligible because dilute salt solutions with negligible osmotic pressures were employed in all the simulations. Consequently, the permeate flux does not change appreciably with axial position in any of these results. Hence, only the mixture composition and membrane surface concentrations of the ions dictate the variability of intrinsic ion rejections.

An interesting observation from the preceding results (Figures 8 and 9) is that the intrinsic rejections of the ions can become independent of the axial position under certain combinations of operating conditions, particularly when the mixture composition and the charge number at the membrane surface becomes constant. Typically, this may happen for

higher fluxes and low shear rates, which induce severe concentration polarization effects. However, it should be kept in mind that this constant intrinsic rejection will not correspond to the bulk electrolyte concentrations in the feed. Instead, the rejections will evolve from a different membrane surface concentration and mixture composition as dictated by the extent of concentration polarization. Hence, even in such cases, use of simplified models of concentration polarization assuming constant intrinsic rejection of the ionic species may yield physically inconsistent and misleading permeate compositions.

Concluding Remarks

A coupled model of concentration polarization and rejection of multicomponent salt mixtures in crossflow nanofiltration systems is developed by simultaneously solving the governing transport equations in the boundary layer adjacent to the membrane and the equations for ion migration through the membrane pores. The predictions of the coupled model provide considerable insight regarding the paramount importance of the salt concentration and the ionic composition of the mixture at the membrane feed solution interface in governing the salt rejection behavior. It is shown that, to accurately predict the permeate solution composition, a rigorous technique for assessment of axial variations in the intrinsic rejection is mandatory. The developed model is capable of predicting the dependence of the intrinsic and observed rejection on a wide variety of fundamental physico-chemical parameters and operating conditions, and we have shown here the influence of a selected number of these parameters. Among these, the membrane charge number and the salt ratio play dominant roles in governing the rejection. Both these dimensionless parameters reflect the influence of membrane surface concentration of the ionic species on the pore transport behavior. Since concentration polarization alters this concentration locally in a crossflow filtration channel, the intrinsic rejection also becomes a local parameter (except under certain limiting conditions). One of the key observations in this study is that operating conditions in a nanofiltration process, for instance, permeate flux and shear rate, will have considerable influence on the intrinsic rejection of the ions. Consequently, the intrinsic separation behavior of a membrane may be controlled by using suitable combinations of operating pressure, channel length, and shear rate.

Acknowledgment

The authors acknowledge the support of the National Science Foundation Research Grant BES-9996240 (formerly BES 9705717).

Notation

c_i = concentration of component i within the membrane
$c_{i,0}$ = concentration of component i just inside the pore entrance
$c_{i,\Delta y}$ = concentration of component i just inside the pore exit
C_i = concentration of ionic component i in the CP layer
$C_{i,b}$ = bulk feed concentration of ionic component i
$C_{i,m}$ = membrane surface concentration of ionic component i
$C_{i,p}$ = bulk permeate concentration
C_T = total bulk salt concentration
Ch = charge number defined by Eq. 19
$D_{i,m}$ = hindered diffusivity within the membrane pore
$D_{i,\infty}$ = bulk (Stokes-Einstein) diffusivity
F = Faraday's constant (96,500 C mol^{-1})
I = current through the membrane
j_i = flux of ionic component i in membrane pore
J_v = permeate flux
$K_{i,c}$ = convective hindrance factor of component i defined by Eq. (11a)
$K_{i,d}$ = diffusivity hindrance factor of component i defined by Eq. (11b)
L_p = membrane permeability
N_A = Avogadro number (6.022×10^{23} mol^{-1})
Pe_i = pore Peclet number
$r_{i,s}$ = radius of ionic component i
r_p = membrane pore radius
R = universal gas constant
$R_{i,\text{int}}$ = intrinsic rejection of component i
$R_{i,\text{obs}}$ = observed rejection
S_i = intrinsic salt passage of component i
T = absolute temperature
u = axial flow velocity
u_i = ionic mobility of component i
x = axial direction along the membrane channel
x_{Cl^-} = chloride ratio in a salt mixture defined in Eq. 18
X = membrane (pore) charge
y = transverse direction from the membrane surface
$Y_{i,p}$ = nondimensionlized membrane concentration
z_i = valence of component i
α = membrane porosity
δ = CP boundary layer thickness
γ = cross-flow shear rate
ΔP = applied pressure
$\Delta\Pi_m$ = transmembrane osmotic pressure difference
$\Delta\psi_D$ = Donnan potential difference across the membrane
η = non-dimensionalized distance, Eq. A.1
λ_i = ratio of radius of component i to pore radius
μ = solvent viscosity
ξ_i = nondimensionalized membrane concentration
σ_o = osmotic reflection coefficient
ϕ_i = partition coefficient defined by Eq. 13
ψ_m = electrical potential in membrane pore

Literature Cited

Basu, S., and M. M. Sharma, "An Improved Space-Charge Model for Flow through Charged Microporous Membranes," *J. Memb. Sci.*, **124**, 77 (1997).

Bhattacharjee, S., A. S. Kim, and M. Elimelech, "Concentration Polarization of Interacting Solute Particles in Cross-Flow Membrane Filtration," *J. Colloid Interf. Sci.*, **212**, 81 (1999).

Bhattacharjee, S., A. Sharma, and P. K. Bhattacharya, "Estimation and Influence of Long Range Solute Membrane Interactions in Ultrafiltration," *Ind. Eng. Chem. Res.*, **35**, 3108 (1996).

Bouchard, C. R., P. J. Carreau, T. Matsuura, and S. Sourirajan, "Modeling of Ultrafiltration—Predictions of Concentration Polarization Effects," *J. Memb. Sci.*, **97**, 215 (1994).

Bowen, W. R., and A. W. Mohammad, "Diafiltration By Nanofiltration—Prediction and Optimization," *AIChE J.*, **44**, 1799 (1998).

Bowen, W. R., and H. Mukhtar, "Characterization and Prediction of Separation Performance of Nanofiltration Membranes," *J. Memb. Sci.*, **112**, 263 (1996).

Cwirko, E. H., and R. G. Carbonell, "Transport of Electrolytes in Charged Pores—Analysis Using the Method of Spatial Averaging," *J. Colloid Interf. Sci.*, **129**, 513 (1989).

Cwirko, E. H., and R. G. Carbonell, "A Theoretical-Analysis of Donnan Dialysis Across Charged Porous Membranes," *J. Memb. Sci.*, **48**, 155 (1990).

De, S., S. Bhattacharjee, A. Sharma, and P. K. Bhattacharya, "Generalized Integral and Similarity Solutions of the Concentration Profiles for Osmotic Pressure Controlled Ultrafiltration," *J. Memb. Sci.*, **130**, 99 (1997).

Deen, W. M., "Hindered Transport of Large Molecules in Liquid-Filled Pores," *AIChE J.*, **33**, 1409 (1987).

Donnan, F. G., "Theory of Membrane Equilibria and Membrane Potentials in the Presence of Non-Dialysing Electrolytes, a Contribution to Physical-Chemical Physiology," *J. Memb. Sci.*, **100**, 45 (1995).

Dresner, L., "Some Remarks on the Integration of the Extended Nernst-Planck Equations in the Hyperfiltration of Multicomponent Solutions," *Desalination*, **10**, 27 (1972).
Elimelech, M., and S. Bhattacharjee, "A Novel Approach for Modeling Concentration Polarization in Crossflow Membrane Filtration Based on the Equivalence of Osmotic Pressure Model and Filtration Theory," *J. Memb. Sci.*, **145**, 223 (1998).
Hall, M. S., V. M. Starov, and D. R. Lloyd, "Reverse Osmosis of Multicomponent Electrolyte Solutions. 1. Theoretical Development," *J. Memb. Sci.*, **128**, 23 (1997).
Hijnen, H. J. M., and J. A. M. Smit, "An Analysis of Partially Film-Controlled Membrane Potentials of Weak Cation Exchange Membranes Using the Space-Charge Model," *J. Memb. Sci.*, **168**, 259 (2000).
Hijnen, H. J. M., J. Vandaalen, and J. A. M. Smit, "The Application of the Space-Charge Model to the Permeability Properties of Charged Microporous Membranes," *J. Colloid Interf. Sci.*, **107**, 525 (1985).
Masliyah, J. H., *Electrokinetic Transport Phenomena*, AOSTRA, Edmonton, Alberta (1994).
Mulder, M., *Basic Principles of Membrane Technology*, Kluwer, Dordrecht (1991).
Palmeri, J., P. Blanc, A. Larbot, and P. David, "Theory of Pressure Driven Transport of Neutral Solutes and Ions in Porous Ceramic Nanofiltration Membranes," *J. Memb. Sci.*, **160**, 141 (1999).
Peeters, J. M. M., J. P. Boom, M. H. V. Mulder, and H. Strathmann, "Retention Measurements of Nanofiltration Membranes with Electrolyte Solutions," *J. Memb. Sci.*, **145**, 199 (1998).
Peeters, J. M. M., M. H. V. Mulder, and H. Strathmann, "Streaming Potential Measurements as a Characterization Method for Nanofiltration Membranes," *Colloids Surf.*, **150**, 247 (1999).
Petzold, L. R., "A Description of DASSL: A Differential/Algebraic System Solver," Sandia National Laboratories, Albuquerque, NM (1982).
Porter, M. C., "Concentration Polarization with Membrane Ultrafiltration," *Ind. Eng. Chem. Prod. Res. Dev.*, **11**, 234 (1972).
Raman, L. P., M. Cheryan, and N. Rajagopalan, "Consider Nanofiltration for Membrane Separation," *Chem. Eng. Prog.*, **3**, 68 (1994).
Saksena, S., and A. L. Zydney, "Influence of Protein-Protein Interactions on Bulk Mass Transport during Ultrafiltration," *J. Memb. Sci.*, **125**, 93 (1997).
Sasidhar, V., and E. Ruckenstein, "Electrolyte Osmosis Through Capillaries," *J. Colloid Interf. Sci.*, **82**, 439 (1981).
Sasidhar, V., and E. Ruckenstein, "Anomalous Effects During Electrolyte Osmosis Across Charged Porous Membranes," *J. Colloid Interf. Sci.*, **85**, 332 (1982).
Smit, J. A. M., "Reverse Osmosis in Charged Membranes: Analytical Predictions from the Space Charge Model," *J. Colloid Interf. Sci.*, **132**, 413 (1989).
Song, L., and M. Elimelech, "Theory of Concentration Polarization in Crossflow Filtration," *J. Chem. Soc. Faraday Trans.*, **91**, 3389 (1995).
Tsuru, T., M. Urairi, S. Nakao, and S. Kimura, "Negative Rejection of Anions in the Loose Reverse-Osmosis Separation of Monovalent and Divalent Ion Mixtures," *Desalination*, **81**, 219 (1991a).
Tsuru, T., M. Urairi, S. Nakao, and S. Kimura, "Reverse-Osmosis of Single and Mixed Electrolytes With Charged Membranes—Experiment and Analysis," *J. Chem. Eng. Jpn.*, **24**, 518 (1991b).
Tsuru, T., S. Nakao, and S. Kimura, "Calculation of Ion Rejection By Extended Nernst-Planck Equation With Charged Reverse-Osmosis Membranes For Single and Mixed Electrolyte-Solutions," *J. Chem. Eng. Jpn.*, **24**, 511 (1991c).
Wang, X., T. Tsuru, S. Nakao, and S. Kimura, "Electrolyte Transport through Nanofiltration Membranes by the Space-Charge Model and the Comparison with Teorell-Meyer-Sievers Model," *J. Memb. Sci.*, **103**, 117 (1995).
Zwillinger, D., *Handbook of Differential Equations,* Academic Press, Chestnut, MA (1989).

Appendix: Numerical Solution of the Pore Transport Equations

The governing equations for pore transport are nondimensionalized using the following scaled variables and parameters

$$\xi_i = \frac{c_i}{c_{i,0}};\ \eta = \frac{y}{\Delta y};\ Y_{i,p} = \frac{C_{i,p}}{c_{i,0}} \quad \text{and} \quad Pe_i = \frac{J_v \Delta y}{D_{i,\infty}} \tag{A1}$$

Combining Eqs. 6 and 9 and employing these scaled variables, the final nondimensional form of the transport equation becomes

$$\frac{d\xi_i}{d\eta} = \frac{Pe_i}{K_{i,d}}\left(K_{i,c}\,\xi_i - Y_{i,p}\right) - z_i\,\xi_i \frac{\sum_i \dfrac{z_i c_{i,0} Pe_i}{K_{i,d}}\left(K_{i,c}\,\xi_i - Y_{i,p}\right)}{\sum_i z_i^2 c_{i,0}\,\xi_i} \tag{A2}$$

with nondimensional boundary conditions

$$\xi_i = 1 \quad \text{at} \quad \eta = 0 \tag{A3}$$

$$\xi_i = \frac{c_{i,\Delta y}}{c_{i,0}} = \frac{\phi_i C_{i,p}}{\phi_i C_{i,m}} = S_i \quad \text{at} \quad \eta = 1 \tag{A4}$$

and pore electroneutrality condition

$$\sum_i z_i c_{i,0}\,\xi_i + X = 0 \tag{A5}$$

The above equations were employed in this study to model transport behavior of three-component mixtures. This was performed by simultaneously solving the coupled ordinary differential equations (Eq. A2) for two of the components to obtain their concentrations in the pores, while the concentration of the third component was obtained using the electroneutrality condition (Eq. A5). The boundary value problem was solved numerically using a shooting technique (Zwillinger, 1989), which entails iterating on the intrinsic salt passage through the membranes

$$S_i = \frac{C_{i,p}}{C_{i,m}} \tag{14}$$

The Powell hybrid technique was used to obtain successive estimates of S_i until convergence, while Gear's predictor-corrector technique was employed to solve the coupled ODEs during each iteration (Zwillinger, 1989). Solution of the pore transport equations yields the intrinsic rejection of the various ionic species according to Eq. 15.

Manuscript received Feb. 12, 2001, and revision received June 13, 2001.